JOURNAL OF PROPULSION AND POWER
Vol. 15, No. 6, November–December 1999

Evaluation of Stored Energy in Ultrafine Aluminum Powder Produced by Plasma Explosion

Jonathan T. DeSena* and Kenneth K. Kuo†
Pennsylvania State University, University Park, Pennsylvania 16802

Ultrafine aluminum powder produced by plasma explosion (ALEX) exhibits burn behavior unlike that of ordinary aluminum powders. Others have previously suggested that the source of this unique behavior might be stored internal energy. The objective of this study is to evaluate theoretically the feasibility of energy being stored in ALEX as a result of work performed by means of the compression of the liquid portion of an ALEX particle by its shrinking solid shell during rapid solidification of the particle. A theoretical model of this process of energy storage was developed. This model was then formulated and numerically solved on a computer for a variety of conditions. Results show that the postulated mechanism results in measurable stored energy for only unrealistically high cooling rates. It is concluded that, although the postulated mechanism could store energy, the amount of energy stored is realistically negligible. This theoretical finding is in agreement with recent experiments that show no observable stored energy in ALEX particles.

Nomenclature

A = surface area, m^2
B = bulk modulus, N/m^2
C_p = specific heat, J/kg · K
D = diameter, m
E_{st} = thermal energy stored during solidification, J
H_f = latent heat of fusion, J/kg
h = heat transfer coefficient, W/m^2 · K
k = thermal conductivity, W/m · K
m = mass, kg
N = surface node
P = pressure, Pa
r = radius, m
T = temperature, K
T_i = initial temperature, K
V = volume, m^3
W = work, J
β = thermal coefficient of expansion, 1/K
Δt = time-step increment, s
ρ = density, kg/m^3

Subscripts

a = ambient
i = inner
l = liquid
m = melting point
n = any node in the sphere
n_s = newest solidified node
o = outer

Superscript

p = time step

Introduction

ULTRAFINE aluminum powder produced by a plasma explosion of wires, called ALEX, possesses characteristics unlike those of ordinary aluminum powder. Ivanov and Tepper[1] found that mixtures of ALEX with various oxidizers yield burning rates many times higher than those of mixtures with ordinary aluminum powder. Mench et al.[2] have confirmed this enhanced burning rate phenomenon of ALEX for several solid propellants and hydroxyl terminated polybutadiene (HTPB) solid fuel. However, the cause for this burning rate increase has not yet been definitively identified.

Using thermal gravimetric analysis (TGA) and differential thermal analysis (DTA) of ALEX, Ivanov and Tepper[1] noted that an exotherm occurred at 450°C and peaked at 550°C without oxidation. From this result, they suggested that the unique burning characteristics of ALEX might be due to a stored internal energy, which is released on reaching a threshold temperature. Ivanov[3] estimated this stored energy to be 400 cal/g (or 1.67×10^6 J/kg).

This claim of stored energy has recently been refuted by several research teams. Mench et al.[2] performed TGA and DTA experiments with ALEX, observing no release of internal energy. Katz et al.[4] used differential scanning calorimetry (DSC) and DTA experiments to arrive at the same conclusion. Before the publication of these findings, the current study commenced with the intent of investigating the possibility that the rapid solidification of aluminum droplets during the plasma explosion process might impart stored internal energy to ALEX. In principle, a highly disordered crystal may contain higher internal energy than the same material in a more ordered crystal structure. Therefore the recrystallization process could be exothermic. According to Ivanov and Tepper,[1] the energy released by recrystallization is too small to produce the unique behavior of ALEX. Thus an alternative source of internal energy was considered.

It was postulated that, during the very rapid cooling of an individual droplet of aluminum, the outer region of the particle would cool faster than the inner region; and if an outer shell solidifies and shrinks as it cools, it may compress the molten liquid in the inner region. This process may perform work on the liquid region and store energy in the particle. Thus the objective of this study is to determine whether measurable energy can in fact be stored in an ALEX particle during the rapid solidification process because of the compression of the inner liquid region by the shrinking outer solid shell or crust.

Method of Approach

The approach taken in this investigation was to 1) develop a theoretical model simulating the cooling, solidification, and shrinkage process of a heated single aluminum droplet; 2) implement a numerical program based on the model formulation; 3) conduct parametric studies with this computer program; and 4) compare calculated results with experimental data.

Received 16 February 1999; revision received 12 May 1999; accepted for publication 14 May 1999.

*Honored Student of Engineering Science of Mechanics.

†Distinguished Professor of Mechanical Engineering and Director of the High Pressure Combustion Laboratory. Fellow AIAA.

Theoretical Model

As described by Ivanov and Tepper,[1] when a very high voltage is applied to the thin aluminum wire over a very short period of time in an inert gas environment, the wire will explode to form numerous nanosized particles. This model considers the event after the initial formation of liquid aluminum particles. Several assumptions, as follow, were made to simplify matters:

1) The original molten aluminum particle after the plasma explosion is spherical and initially has a uniform temperature.

2) In view of its extremely small size (average diameter ~100 nm), the particle is cooled uniformly over its surface.

3) The subsurface temperature profile is a function of time and radius only.

4) Heat transfer inside the droplet is due to conduction only; no internal circulation occurs within the liquid.

5) Solidification begins on the external surface and proceeds uniformly inward to the center as a spherical shell.

6) Solidification begins when the material is cooled to its melting temperature of 933.5 K—no undercooling.

7) Solidifying material maintains the melting temperature until completely solidified.

8) There is no sublimation. The aluminum goes through each phase along the way to becoming a solid.

9) Liquid aluminum is compressible.

10) The liquid will not shrink as a result of cooling.

11) Solid aluminum is inelastic at all temperatures below the solidification point, such that a stress will not result in a deformation or fracture. This assumption is required for eliminating the indeterminate nature of the shrinking phenomenon; without it, it cannot be known how much a solid node bounded by other solid nodes will shrink.

12) ALEX particle manufacturing process is performed in an inert gas (argon) environment. Also, the passivation process does not relieve any energy stored by the shrinking process. Therefore, no consideration of an oxide layer is included in the analysis.

While these assumptions are not absolutely accurate representations of physical reality, they are necessary for simplification of the mathematics, and most of them are quite reasonable.

In what follows, the theoretical model and the numerical scheme are described together. For convenience of model description, the nodal setup is introduced first. The one-dimensional nodal network for this finite-difference method was set up as follows (see Fig. 1):

1) One node is always on the particle surface, called node N.

2) One node is always at the center, called node 1.

3) All other nodes are initially evenly spaced between the surface and the center nodes. Interior nodes are numbered sequentially.

4) The inner radius of node n is defined as the midpoint between nodes n and $n-1$. The outer radius of node n is defined as the midpoint between nodes n and $n+1$. The inner radius of node n therefore is the same as the outer radius of node $n-1$.

5) Nodal mass of each node is defined to be the spherical shell between its inner and outer radii. This mass is assumed constant throughout the calculations and is always identified with the same node.

The initial density of the particle was estimated with the initial temperature in a linear temperature–density relationship.[5] In the analysis and calculations, the thermal conductivity k, specific heat C_p, and thermal expansion coefficient β, are treated as temperature-dependent parameters through a linear interpolation scheme. Data for the values used in interpolation were taken from the *Handbook of Physical Quantities*.[6]

Noting that the stability requirements for the explicit finite-difference formulation would require so many time steps as to be computationally inefficient, we therefore selected an implicit approach. For solving the subsurface temperature profile, implicit finite-difference equations for the temperature of a node at a particular time step T_n^p can be derived with the energy-balance method on the node over that time step. These equations are derived for three cases of nodal locations: the center node (case 1), the interior node (case 2), and the surface node (case 3). For each case, the physical

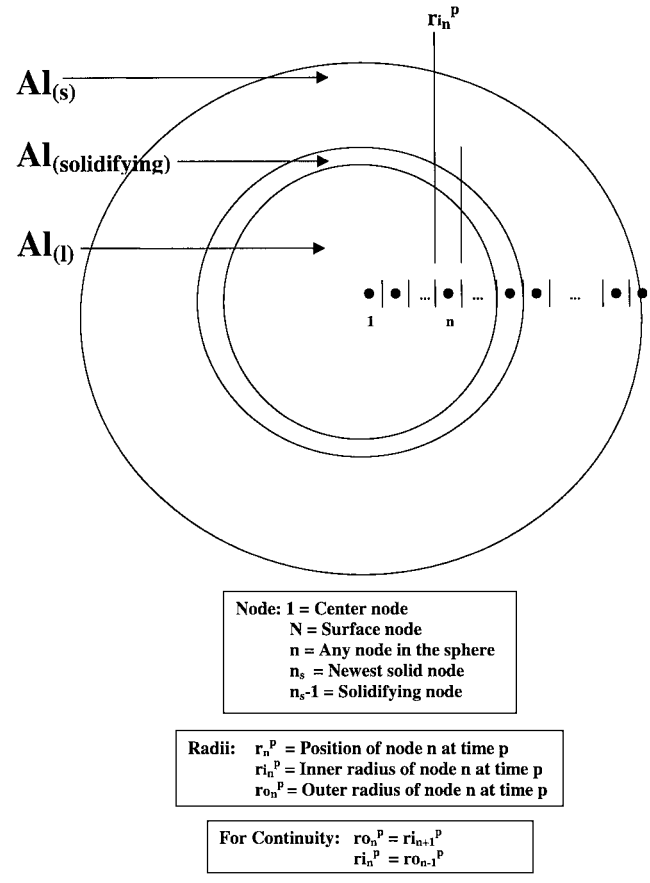

Fig. 1 Nodal setup for the theoretical model.

differential equation is given first, followed by the resulting implicit finite-difference temperature equation.

Case 1: For the center node there is conduction of energy only out of the node. In this case, $n = 1$:

$$\rho V C_p \frac{\partial T}{\partial t} = -\left(kA\frac{\partial T}{\partial r}\right)_{\text{out}} \tag{1}$$

$$T_1^p = \frac{\left[-k_{o_1}A_{o_1}\Delta t \big/ \rho_1 V_1 C_{p_1}(r_2 - r_1)\right]T_2^p + T_1^{p-1}}{1 + \left[-k_{o_1}A_{o_1}\Delta t \big/ \rho_1 V_1 C_{p_1}(r_2 - r_1)\right]} \tag{2}$$

Case 2: For an interior node there is conduction into and out of the node. In this case $1 < n < N$:

$$\rho V C_p \frac{\partial T}{\partial t} = -\left(kA\frac{\partial T}{\partial r}\right)_{\text{in}} + \left(kA\frac{\partial T}{\partial r}\right)_{\text{out}} \tag{3}$$

$$T_n^p = \left(\frac{\rho_n V_n C_{p_n}}{\Delta t}T_n^{p-1} + \frac{k_{i_n}A_{i_n}}{r_n - r_{n-1}}T_{n-1}^p + \frac{k_{o_n}A_{o_n}}{r_{n+1} - r_n}T_{n+1}^p\right)\Bigg/ \left(\frac{\rho_n V_n C_{p_n}}{\Delta t} + \frac{k_{i_n}A_{i_n}}{r_n - r_{n-1}} + \frac{k_{o_n}A_{o_n}}{r_{n+1} - r_n}\right) \tag{4}$$

Case 3: For the surface node, energy flux enters by means of conduction and exits by means of convection. In this case $n = N$:

$$\rho V C_p \frac{\partial T}{\partial t} = -\left(kA\frac{\partial T}{\partial r}\right)_{\text{in}} + hA_{\text{out}}(T_a - T_{\text{surface}}) \tag{5}$$

$$T_N^p = \left(\frac{k_{i_N}A_{i_N}}{r_N - r_{N-1}}T_{N-1}^p + hA_{o_N}T_a + \frac{\rho_N V_N C_{p_N}}{\Delta t}T_N^{p-1}\right)\Bigg/ \left(\frac{k_{i_N}A_{i_N}}{r_N - r_{N-1}} + hA_{o_N} + \frac{\rho_N V_N C_{p_N}}{\Delta t}\right) \tag{6}$$

These equations are applicable as long as the node is not solidifying. If the node is solidifying, the node temperature is set to the melting temperature, i.e.,

$$T_n^p = T_m \tag{7}$$

It should be noted that these equations assume a constant product of $\rho V C_p$ over a time step. Both the density and the volume may change from time step to time step but the product of the two, the mass, remains constant. The specific heat is calculated as a function of temperature and can change over time as the temperature changes. This may seem to present a problem, but if the specific heat changes only slightly then the equations should remain accurate.

For an interior node, $1 < n < N$, the rate of thermal energy storage is the difference between the energy flux entering the node by conduction and the energy flux leaving the node by conduction as described by Eq. (8). When a node reaches the melting temperature, the node is said to be solidifying. At this point, the net amount of thermal energy leaving this node over each time step is calculated from Eq. (9), the implicit finite-difference equation based on Eq. (8):

$$\dot{E}_{\text{st}} = -\left(kA\frac{\partial T}{\partial r}\right)_{\text{in}} + \left(kA\frac{\partial T}{\partial r}\right)_{\text{out}} \tag{8}$$

$$E_{\text{st}_n}^p = \left[k_{i_n}A_{i_n}\frac{T_{n-1}^p - T_n^p}{r_n - r_{n-1}} - k_{o_n}A_{o_n}\frac{T_n^P - T_{n+1}^p}{r_{n+1} - r_n}\right]\Delta t \tag{9}$$

For the center node, simply eliminate the first term on the right-hand side of Eq. (9), as there is only conductive energy flux leaving the node. For the surface node, the second term on the right-hand side of Eq. (9) is replaced with $-hA_o(T_n^p - T_a)$ as the energy flux leaving the node is due to convection.

When the thermal energy storage summed over a period of time from the beginning of solidification to the current time just reaches or exceeds the energy loss required for solidification (the product of the mass of the node and the latent heat of fusion of aluminum), then the node is considered solidified.. This condition for solidification can be represented mathematically by

$$\sum_{i=p_m}^{p} E_{\text{st}_{n_s}}^i \geq m_{n_s} H_f \tag{10}$$

where p represents the current time step and p_m is the time step when solidification begins. The value for latent heat of fusion[7] for aluminum used in this experiment is $H_f = 3.97 \times 10^5$ J/kg. Thereafter, the node is again permitted to drop in temperature.

To calculate the compression work performed on the liquid by the solidified solid shell, the shrinkage of the solid must first be calculated. This means that the radius change of solid nodes that is due to cooling must be determined. The linear thermal expansion coefficient β is defined as the percentage of radius change with respect to temperature change, i.e.,

$$\beta \equiv (1/r)(\Delta r/\Delta T) \tag{11}$$

For the most recently solidified node n_s, the outer and the inner radii of the node are altered with Eqs. (12) and (13), respectively:

$$r_{o_{n_s}}^p = r_{o_{n_s}}^{p-1}\beta\left(T_{n_s}^p - T_{n_s}^{p-1}\right) + r_{o_{n_s}}^{p-1} \tag{12}$$

$$r_{i_{n_s}}^p = r_{i_{n_s}}^{p-1}\beta\left(T_{n_s}^p - T_{n_s}^{p-1}\right) + r_{i_{n_s}}^{p-1} \tag{13}$$

The radial location of the n_s node can be calculated from

$$r_{n_s}^p = \begin{cases} \dfrac{r_{o_{n_s}}^p + r_{i_{n_s}}^p}{2}, & 0 < n_s < N \\ 0, & n_s = 1 \\ r_{o_{n_s}}^p, & n_s = N \end{cases} \tag{14}$$

After the radii of the n_s node are changed, the radii of all the other nodes must be adjusted accordingly. The nodes in the liquid region are spaced evenly. The displacement of the solid nodes are based upon the mass continuity, which requires that

$$r_{i_n}^p = r_{o_{n-1}}^p \tag{15}$$

Because the solid cannot be compressed, the mass continuity implies the volume constancy of the nodes in the solid region. When the inner radius of node n, which was determined from Eq. (15), is known, the outer radius can be calculated for any solid node n based on the assumption that the volume of the solidified shell remains constant, i.e.,

$$r_{o_n}^p = 3\sqrt{\left(r_{o_n}^{p-1}\right)^3 - \left(r_{i_n}^{p-1}\right)^3 + \left(r_{i_n}^p\right)^3} \tag{16}$$

The preceding instantaneous radius information is used for determining the work done by the shrinking solid shell on the liquid. Summing this work over time results in an estimate for the energy stored in an ALEX particle by this mechanism. The work done over a particular time step can be calculated as the product of the pressure in the liquid and the change in the volume of the liquid over the time step:

$$W_l^p = P_l^p\left(V_l^{p-1} - V_l^p\right) \tag{17}$$

To calculate the pressure in the liquid, the definition of the bulk modulus B is used:

$$B = -\frac{\Delta P}{(\Delta V/V)} \tag{18}$$

Solving this equation for the pressure and substituting into Eq. (17) result in the final work equation:

$$W_l^p = \left(-B\frac{V_l^p - V_l^{p-1}}{V_l^{p-1}} + P_i^{p-1}\right)\left(V_l^{p-1} - V_l^p\right) \tag{19}$$

The change in the volume of the liquid is calculated such that only the volume change that is due to the compression by the solid shell is reflected. It should be noted that the liquid volume change that is due to the solidification of a node (which changes the mass and volume of the liquid) is not considered a part of volume change because of compression. Also, note that compressive work, as is done by the shrinking of the solid shell, is treated as positive work.

It seems that the bulk modulus (the reciprocal of the compressibility) is not a known value for liquid aluminum. To use this method, a reasonable estimate must be made. For solid aluminum, the bulk modulus[7] is approximately 7×10^{10} N/m^2. The bulk modulus for liquid aluminum must be somewhat lower than this value. For comparison with a liquid metal whose value is known, the bulk modulus of mercury[7] is approximately 2.8×10^{10} N/m^2. Perhaps the bulk modulus of liquid aluminum is approximately this value; at least it should be of the order of 10^{10} N/m^2. For the purposes of this investigation the bulk modulus of liquid aluminum is taken to be 2×10^{10} N/m^2.

In view of assumptions 10 and 11, the calculated work represents a maximum possible work by the outlined model and procedure. Assumption 10 demands that the compression of the liquid by the solid shell be larger than it would be if the liquid were allowed to shrink on its own because of cooling. Assumption 11 eliminates any energy lost because of deformations of the solid.

Solution Procedure

The numerical analysis and computational procedure solve the following physical quantities in sequence for each time step: 1) subsurface temperature profile, 2) location of the solidification front, 3) radii changes for all nodes, and 4) work done on the liquid by the shrinkage of the solidified aluminum shell. The computer code was implemented in FORTRAN 77.

The code was tested against several known analytical solutions. The calculated instantaneous temperature profiles of a sphere cooled

by convection under a constant heat transfer coefficient were found to be in extremely close agreement with the analytical solution given in an infinite series in Ref. 8. The analytical solution was evaluated with the first 20 terms of the series. The higher-order terms were found to be truly negligible. The computer code was also tested against a known solution to a solidification problem. Calculated total time for solidification of a highly conductive sphere was also in very close agreement (differing by only 0.07%) with that of a lumped parameter analysis for a sphere with extremely low values of Biot number. Under such conditions, the temperature profile inside the sphere can be considered uniform in the analytical solution.

Nodal Analysis

The effect of the number of nodes on the calculated solution was also tested with several different numbers of nodes. This was performed for two different heat transfer coefficients at the particle surface ($h = 2 \times 10^7$ and 2×10^{10} W/m$^2 \cdot$ K), covering a wide range of Biot numbers. The calculated temperature profiles and the work values were compared for different numbers of nodes. It was found that the calculated temperature profiles for 20 and 40 nodes at both heat transfer coefficients were essentially the same. The calculated work showed the tendency to reach an asymptotic value as the number of nodes was increased from 10 to 40 with an increment of 10 nodes. The higher the heat transfer coefficient, the smaller the percent difference between the solutions with 30 and 40 nodes. The work value increased 6.5% from 30 to 40 nodes. Compromising the solution accuracy with computation time, the 30-node pattern was selected for the rest of the calculations.

The program was executed in a DOS box on a 233-MHz Pentium II IBM compatible machine with 32-MB RAM running Windows 95 for a variety of cases. For each case the time-step increment size was reduced until the change in the results from one time step to the next was minimal, meanwhile allowing enough time for the calculations to be completed. In general, the time steps used in computation are of the order of 10^{-14} s.

Discussion of Results

Because of the uncertainties following the high-voltage-induced plasma explosion process for particle generation, the program was executed under a broad range of conditions, varying the following parameters: 1) the heat transfer coefficient h during the cooling and solidification processes, 2) the ambient pressure of the inert gas environment P_a, and 3) the initial temperature of the particle T_i.

The ambient temperature of the inert gas in each case was set to 300 K, which is assumed to be the ambient gas temperature before the plasma explosion process. Unless otherwise noted, the initial starting temperature of the sphere was set to 2000 K and the ambient pressure to 1 atm. The initial ALEX particle diameter for each case was set to be 100 nm. The bulk modulus of the liquid aluminum was kept at the preceding estimate of 2×10^{10} N/m^2 for all cases.

The program was executed for several cases of different heat transfer coefficients, chosen to represent a broad range of initial Biot numbers. Only two cases are shown here to keep within paper-length restrictions. The heat transfer coefficients, along with the corresponding Biot number and the time-step increment Δt, used in the calculations, follow:

Case 1:

$$h = 2 \times 10^9 \text{ W/m}^2 \cdot \text{K}, \qquad \text{Bi} = 1, \qquad \Delta t = 1 \times 10^{-14} \text{ s}$$

Case 2:

$$h = 2 \times 10^{10} \text{ W/m}^2 \cdot \text{K}, \qquad \text{Bi} = 10, \qquad \Delta t = 1 \times 10^{-15} \text{ s}$$

Note that the values for h are extremely high in comparison with normally observed heat transfer coefficients. Examining conditions that correspond to Biot numbers much less than 0.1 would not be beneficial, because for such cases the temperature inside the sphere would be practically uniform.

The corresponding figures for each case are arranged in a set of three graphs, including the time variation of temperature profiles, the work done at each time step, and the total work done per unit mass of the particle. The case 1 results are shown in Figs. 2–4. The case 2 results are shown in Figs. 5–7. In each of the temperature

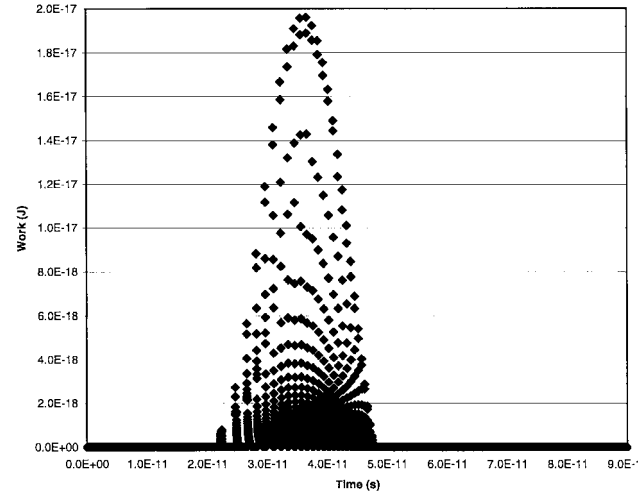

Fig. 3 Incremental work done on liquid by a solid shell for h = 2.0×10^9 W/m$^2 \cdot$ K.

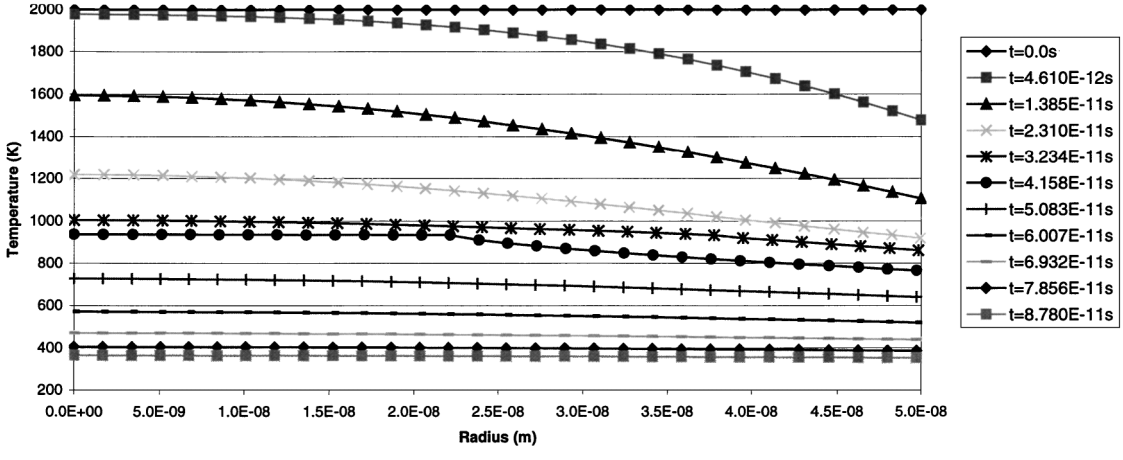

Fig. 2 Subsurface temperature profiles of aluminum particle with initial diameter D = 100 nm cooled uniformly over its surface with a total heat transfer coefficient h = 2.0×10^9 W/m$^2 \cdot$ K and ambient temperature T_a = 300 K.

graphs the temperature profile is given for 11 different times during the cooling; the difference between sequential times is constant from the second (from the top) through eleventh curves. When examining the temperature graphs, note that the melting temperature of aluminum is $T_m = 933.5$ K, at which the temperature profiles exhibit slope discontinuity. For the higher heat transfer case (case 2), the temperature profiles are less uniform than those of case 1 because of more rapid heat loss to the surrounding gas. The slope discontinuity at the melting temperature is also more pronounced than that in case 1. Also, the particle cools to the same temperature in a much shorter time.

The work done on the liquid by the shrinking of the solid spherical shell is shown as the amount of work performed over each individual time-step increment in Figs. 3 and 6 for cases 1 and 2, respectively. Each point on these two graphs represents the work done over the particular time step that occurs at the corresponding time. The total work per unit mass that has been performed on the liquid by the solid shell up to the current time is illustrated in Figs. 4 and 7 for cases 1 and 2, respectively. These graphs show the sum of the incremental work done per unit mass at each time step up to the current time. These curves are akin to the integral of the incremental work per unit mass; however, they are not technically the area integrals of Figs. 3 and 6 because they are really sums of heights. The reasons for the bell-shaped boundaries of Figs. 3 and 6 and the ramp rise form of Figs. 4 and 7 are discussed later.

The characteristic "lumps" in the graphs of the total work per unit mass (Figs. 4 and 7) are directly related to the nearly vertical "columns" in the corresponding incremental work graphs shown in Figs. 3 and 6. These so-called columns are not true columns—the points are not multivalued—but this is the easiest way to describe these formations. The columns (and resulting lumps) are products of the nodal numerical analysis. Each column represents the work performed by a particular shrinking node n_s. Most columns can be resolved into two different regions, divided by the point at which the slope is discontinuous. (See Fig. 6 for the best example of this.) The upper region represents the times when the liquid to the inside of the newest solidified node n_s is entirely above the melting temperature. The discontinuity occurs at the time step at which the node $n_s - 1$ has reached the melting point and begins to solidify. The region below the slope discontinuity represents the times when the node $n_s - 1$ is solidifying and remains at the melting temperature. The lowest point in the column is when the node $n_s - 1$ has completed solidification. This node now becomes the new

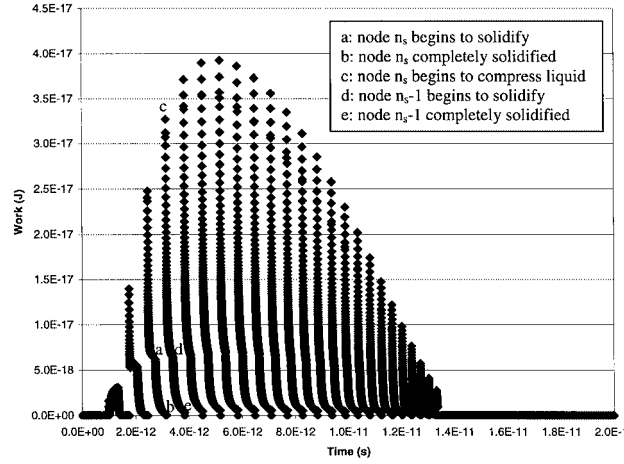

Fig. 6 Incremental work done on liquid by a solid shell for $h = 2.0 \times 10^{10}$ W/m$^2 \cdot$ K.

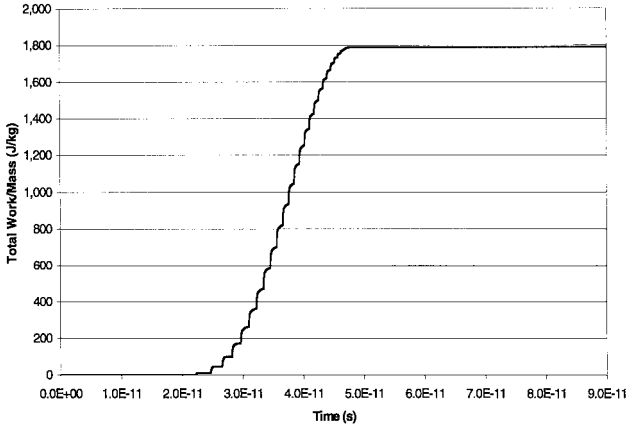

Fig. 4 Total work done per unit mass on liquid by solid shell for $h = 2.0 \times 10^{9}$ W/m$^2 \cdot$ K.

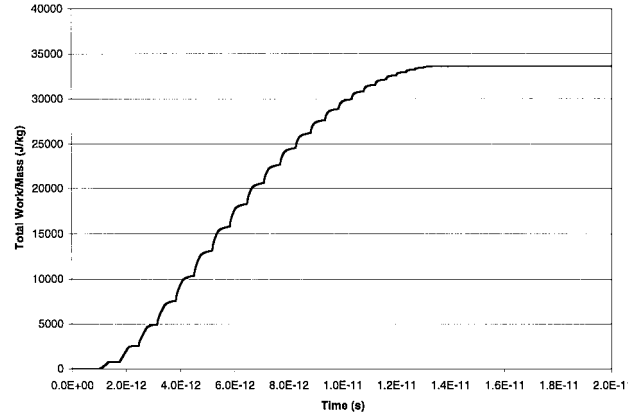

Fig. 7 Total work done per unit mass on liquid by a solid shell for $h = 2.0 \times 10^{10}$ W/m$^2 \cdot$ K.

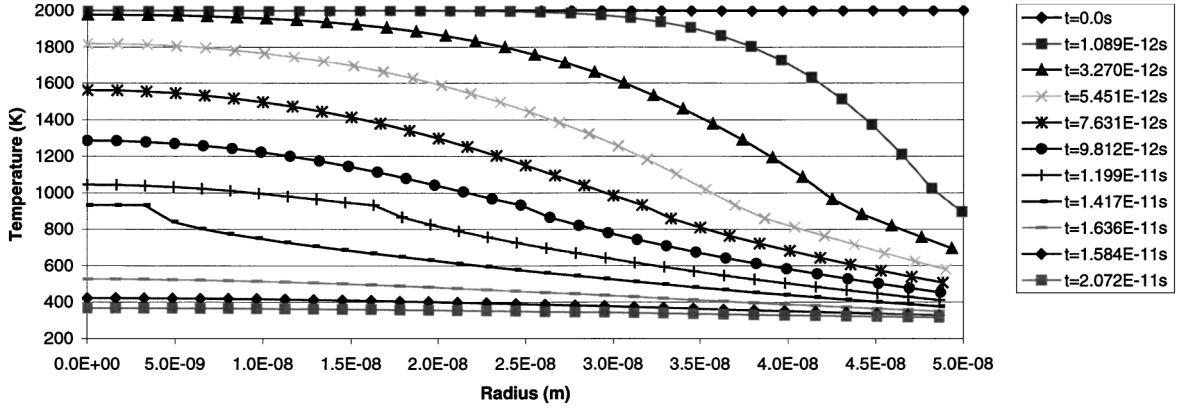

Fig. 5 Subsurface temperature profiles of aluminum particle with initial diameter $D = 100$ nm cooled uniformly over its surface with a total heat transfer coefficient $h = 2.0 \times 10^{10}$ W/m$^2 \cdot$ K and ambient temperature $T_a = 300$ K.

shrinking node, n_s, performing work on the liquid; then a new column starts.

Regarding the detailed shape of the column, the reason for the decrease of work in each column can be explained as follows. As the node n_s is cooled after its solidification, the temperature drop of this node decreases with each time step. This results in the decrease of the radial shrinkage of the node at each time step. As a consequence, the work performed on the liquid aluminum in the interior region is reduced at each time step. This process continues until the node $n_s - 1$ completes solidification. Also, each new column begins at a much higher point than the last point in the previous column, as the node that is now shrinking $n_s - 1$ remains at the melting temperature during its solidification while the outer nodes continue to cool. Thus, during solidification, the temperature gradient between this node and the outer nodes increases. As soon as the material represented by the node $n_s - 1$ is solid, it becomes the new shrinking node n_s and is again permitted to decrease in temperature. At the first time step, when it begins to shrink, it cools more rapidly than at later times because of the high-temperature gradient induced during its solidification. This explains the repetitive column formation.

The bell-shaped boundary of the time variation of incremental work done (see Figs. 3 and 6) can be explained as follows. As the liquid is compressed, the pressure builds up. Thus, as time advances, the pressure term in Eq. (17) grows. As the sphere solidifies, the liquid portion becomes smaller, resulting in smaller volume changes. This volume change term in the work equation counteracts the increasing pressure term. These two counteracting terms result in the bell-shaped boundary of the incremental work graphs. The pressure term increases the work done, dominating the earlier phase of the solidification process; the volume change term tends to reduce the work done and dominates the later phase of the solidification process. The overall ramp rise shape of the total work per unit mass graphs (Figs. 4 and 7) is a direct result of the bell-shaped boundary of the incremental work graphs. The most important output of the calculation is the final sum of work done on the liquid aluminum during particle solidification. This total work can be regarded as the stored excess internal energy in the ALEX particle.

The effect of the heat transfer coefficient on the total work done per unit mass (or stored excess internal energy per unit mass) during solidification by the solid shell on the liquid is illustrated by Fig. 8. As expected, higher heat transfer coefficients result in more work being performed on the liquid. Examination of Fig. 8 reveals that the work per unit mass is of consequential magnitude only when the heat transfer coefficient is extremely high. For intensive purposes, total work per unit mass for heat transfer coefficients below 1×10^8 W/m$^2 \cdot$ K is negligible. Therefore, under realistic heat transfer rates—far lower than those considered in this investigation—the stored excess internal energy of ALEX particles is negligible. Also, it is evident from Fig. 8 that the total work per unit mass asymptotically approaches a level of $\sim 10^5$ J/kg. Thus the maximum work per unit mass appears to be at least an order of magnitude below the 1.67×10^6 J/kg (400 cal/g) initially estimated by Ivanov.[3]

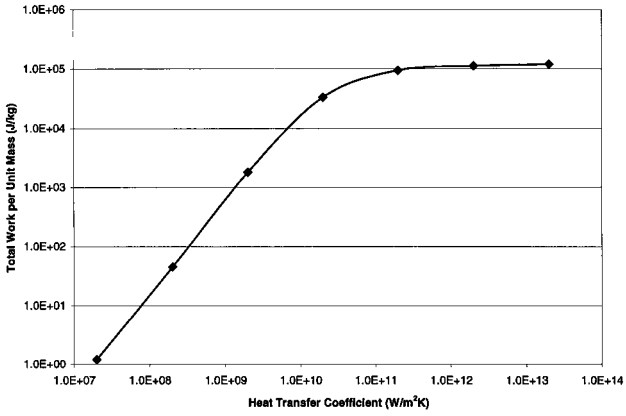

Fig. 8 Effect of heat transfer coefficient on the total work done per unit mass on the liquid by the solid shell.

Table 1 Effect of ambient pressure on total work per unit mass

h, W/m$^2 \cdot$ K	Pressure, atm	1	4	8
2×10^8	Work, J/kg	45.4	45.7	46.1
	Percent change from work at 1 atm	0	0.632	0.838
2×10^{10}	Work, J/kg	33,618	33,628	33,641
	Percent change from work at 1 atm	0	0.029	0.039

Table 2 Duration of compression at each liquid pressure level for the case of $h = 2 \times 10^{10}$ W/m$^2 \cdot$ K and $P_a = 8$ atm

Order of liquid pressure, MPa	1	10	100	1,000
Time duration, 10^{-12} s	0.011	0.105	2.767	17.948

Table 3 Effect of initial particle temperature on the total work per unit mass

h, W/m$^2 \cdot$ K	2×10^7	2×10^8	2×10^9	2×10^{10}
$T_i = 2000$ K	1.203 J/kg	45.43 J/kg	1790 J/kg	33619 J/kg
$T_i = 2700$ K	1.214 J/kg	48.36 J/kg	1896 J/kg	37536 J/kg

The effect of ambient gas pressure on the total excess energy storage per unit mass was studied for the three different chamber pressures at 1, 4, and 8 atm. This parametric study was performed with heat transfer coefficients of 2×10^8 and 2×10^{10} W/m$^2 \cdot$ K. Table 1 illustrates the change in the total work per unit mass that is due to a change of the ambient pressure at each of the two heat transfer coefficients. Based on the parametric study results, the pressure has practically an insignificant effect on the total excess energy storage per unit mass. In addition, the percent increase is smaller for larger heat transfer coefficients, which are the only cases that might provide enough work to store additional energy into ALEX particles.

The small difference for varying pressure is expected because the ambient pressure is very small compared with the pressure exerted by the shrinking shell. Table 2 helps to illustrate this fact. The initial pressure in the liquid is of the order of 0.1 MPa. As soon as shrinking begins the pressure in the liquid jumps to an order of 1 MPa. As Table 2 shows, most of the time during which compression work is being done, the pressure is several orders of magnitude greater than the initial pressure. Similar results are obtained for other cases as well. Therefore, when the heat transfer coefficient is already varied independently, the initial chamber pressure would not be expected to have much effect on the final work value.

The effect of the initial particle temperature on the total excess energy storage was studied in a parametric analysis. Table 3 compares the total work done per unit mass for two different initial temperatures at 2000 and 2700 K (slightly below the boiling point of aluminum) for several heat transfer coefficients. Results show that an increase in the initial temperature results in a slight increase in the total work per unit mass. At higher heat transfer coefficients the increase is more noticeable. At higher initial particle temperatures, the temperature gradients during the solidification and cooling processes are steeper, inducing greater compression work. Nevertheless, this effect is not strong enough to make significant differences in estimates of the excess energy storage in the particle.

Equation (19) can be utilized to determine the effect of the bulk modulus on the instantaneous work and ultimately the amount of excess energy storage. Examination of this equation reveals that the largest change in the instantaneous work is one that is directly proportional to the bulk modulus term. Thus, high-end estimates of the effect of varying the bulk modulus can be made by multiplying the calculated work by the ratio of $B_{\text{new}}/B_{\text{used}}$, where $B_{\text{used}} = 2 \times 10^{10}$ N/m^2.

The bulk modulus of solid aluminum is approximately 7×10^{10} N/m^2. The maximum bulk modulus for liquid aluminum possible, then, is less than this value. To estimate the maximum possible work done, the maximum work calculated in this study was multiplied by the ratio of $B_{\text{new}}/B_{\text{used}} = \frac{7}{2}$. Figure 8 reveals the most liberal estimate of the total work per unit mass possible with

this study, 1×10^5 J/kg. Multiplying this value by $\frac{7}{2}$ gives the maximum work per unit mass of 350,000 J/kg. Even if it were possible, this estimate still lies an order of magnitude below that of Ivanov.[3] In addition, the higher B becomes, the less realistic assumption 11 becomes, as higher B values result in greater pressure in the liquid and correspondingly greater forces on the solid shell.

The current finding of insignificant amount of excess internal energy in the ALEX particle is in agreement with the recent experimental work conducted by Mench et al.,[2,9] Katz et al.,[4] and Ismail and Hawkins.[10] In their DTA studies,[2] no release of internal energy was observed for both fresh and aged batches of ALEX. The regular aluminum powder and ALEX in a helium environment showed no difference in their DTA traces.[9] Katz et al.[4] did not observe any anomalous thermal behavior of ALEX below the oxidation temperature of aluminum, similar to the findings of Refs. 2 and 9. The enhancement of the mass burning rate of solid propellant by the addition of ALEX particles is believed to be due to rapid consumption of ultrafine ALEX particles in the close vicinity of the burning propellant surface.[9] The large specific surface area of ALEX also contributes significantly to the enhanced burning rate of propellants.[9,10] Also, the significant increase in the surface-to-binder contact area was suggested as the reason for the enhanced burning rate phenomenon of ALEX-containing solid propellants.[11] The ignition and combustion behavior of aluminum particles of the order of 20 μm has been studied by Foelsche et al.[12] under high-pressure and high-temperature conditions. Longer ignition delay was observed for much larger particles of the order of 50 μm. The use of the much smaller aluminum particle size is definitely beneficial for achieving shorter ignition delay and more complete combustion.

Conclusions

The work of this investigation leads to the following conclusions:

1) According to the theoretical model described herein, the proposed method of excess energy storage can store some energy only if the heat transfer rate is many orders of magnitude higher than ordinary heat transfer rates.

2) At ordinary heat transfer rates, the stored energy is found to be negligible. This is true even at heat transfer coefficients well above what is generally considered ordinary. Energy storage is significant only for coefficients greater than approximately 10^9 W/m$^2 \cdot$ K. Considering that such values are highly unlikely, any energy realistically stored is negligible.

3) The recent experiments performed by Mench et al.,[2,9] Katz et al.,[4] Ismail and Hawkins,[10] and Bach et al.[11] are confirmed by this theoretical study. Their conclusion that there is in fact no measurable stored energy is in agreement with the finding of negligible excess stored energy in this investigation.

Suggested Future Work

It is useful to note that the approach used by the authors can be considered as a macroscopic one, which does not address the microscopic details of lattice defects in the aluminum crystals. To study the plastic energy storage associated with lattice defects, one could use experimental methods such as x-ray diffraction techniques, x-ray Topography, and transmission electron microscope analysis. The experimental work to study lattice defects is beyond the scope of this paper and should be considered for future studies.

Acknowledgments

A portion of this work was funded through Richard S. Miller of the Mechanics and Energy Conversion Standards and Technology Division of the U.S. Office of Naval Research under Grant N00014-96-1-0785. Communications with Fred Tepper of the Argonide Corporation and Gennady Ivanov of the Institute of Petroleum Chemistry of the Russian Academy of Sciences were highly beneficial to this study.

References

[1]Ivanov, G. V., and Tepper, F., "'Activated' Aluminum as a Stored Energy Source for Propellants," *Challenges in Propellants and Combustion 100 Years After Nobel*, edited by K. K. Kuo et al., Begell House, New York, 1997, pp. 636–645.

[2]Mench, M., Yeh, C., and Kuo, K., "Propellant Burning Rate Enhancement and Thermal Behavior of Ultra-Fine Aluminum Powders (ALEX)," *Energetic Materials Production, Processing and Characterization*, Fraunhofer Institut Chemische Technologie, Karlsruhe, Germany, 1998, pp. 30-1–30-15.

[3]Ivanov, G., "Uniformity of Burning and Detonation of Pyrotechnic Mixtures Based on Activated Aluminum," *1995 JANNAF Propulsion Meeting*, CPIA Pub. 630, Vol. 1, 1995, pp. 89–95.

[4]Katz, J., Tepper, F., Ivanov, G., Lerner, M., and Davidovich, V., "Metastable Nanosize Aluminum Powder as a Reactant in Energetic Formulations," *JANNAF Propulsion Meeting*, CPIA Pub. 675, Vol. 3, 1998, pp. 343–349.

[5]Iida, T., and Guthrie, R., *The Physical Properties of Liquid Metals*, Clarendon, Oxford, England, 1988, pp. 70–91, 188, 189, 233–241.

[6]Grigoriev, I. S., and Meilikhov, E. Z., eds., *Handbook of Physical Quantities*, CRC Press, New York, 1997, pp. 258–260, 313, 314, 421, 422.

[7]Serway, R., *Physics for Scientists and Engineers with Modern Physics*, 3rd ed., Saunders College, Philadelphia, PA, 1992, pp. 310, 533.

[8]Incropera, F., and Dewitt, D., *Fundamentals of Heat and Mass Transfer*, 4th ed., Wiley, New York, 1996, pp. 229, 230.

[9]Mench, M. M., Kuo, K. K., Yeh, C. L., and Lu, Y. C., "Comparison of Thermal Behavior of Regular and Ultra-Fine Aluminum Powders (ALEX) Made from Plasma Explosion Process," *Combustion Science and Technology*, Vol. 135, 1998, Special Issue, pp. 269–292.

[10]Ismail, I. M. K., and Hawkins, T. W., "Evaluation of Electro Exploded Aluminum (ALEX) for Rocket Propulsion," *1996 JANNAF Propulsion Meeting*, CPIA Pub. 650, Vol. 2, 1996, pp. 25–39.

[11]Bach, D. T., Hawkins, T. W., and Brand, A. J., "The Effect of Aluminum Type on Solution Propellant Characteristics," *1996 JANNAF Propulsion Meeting*, CPIA Pub. 650, Vol. 2, 1996, pp. 569–578.

[12]Foelsche, R. O., Burton, R. L., and Krier, H., "Ignition and Combustion of Aluminum Particles in $H_2/O_2/N_2$ Combustion Products," *Journal of Propulsion and Power*, Vol. 14, No. 6, 1998, pp. 1001–1008.